ACS SENSORS

pubs.acs.org/acssensors

Article

A Point-of-Care Immunosensor Based on a Quartz Crystal Microbalance with Graphene Biointerface for Antibody Assay

Piramon Hampitak, Thomas A. Jowitt, Daniel Melendrez, Maryline Fresquet, Patrick Hamilton, Maria Iliut, Kaiwen Nie, Ben Spencer, Rachel Lennon, and Aravind Vijayaraghavan*

Cite This: *ACS Sens.* 2020, 5, 3520−3532

Read Online

ACCESS | Metrics & More | Article Recommendations | Supporting Information

ABSTRACT: We present a sensitive and low-cost immunoassay, based on a customized open-source quartz crystal microbalance coupled with graphene biointerface sensors (G-QCM), to quantify antibodies in undiluted patient serum. We demonstrate its efficacy for a specific antibody against the phospholipase A2 receptor (anti-PLA2R), which is a biomarker in primary membranous nephropathy. A novel graphene−protein biointerface was constructed by adsorbing a low concentration of denatured bovine serum albumin (dBSA) on the reduced graphene oxide (rGO) sensor surface. The dBSA film prevents the denaturation of the protein receptor on the rGO surface and serves as the cross-linker for immobilization of the receptor for anti-PLA2R antibodies on the surface. The detection limit and selectivity of this G-QCM biosensor was compared with a commercial QCM system. The G-QCM immunoassay exhibited good specificity and high sensitivity toward the target, with an order of magnitude better detection limit (of 100 ng/mL) compared to the commercial system, at a fraction of the cost and with considerable time saving. The results obtained from patient sera compared favorably with those from enzyme-linked immunosorbent assay, validating the feasibility of use in clinical applications. The multifunctional dBSA-rGO platform provides a promising biofunctionalization method for universal immunoassay and biosensors. With the advantages of inexpensive, rapid, and sensitive detection, the G-QCM sensor and instrument form an effective autoimmune disease screening tool.

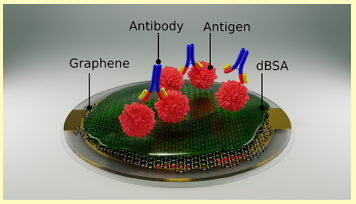

KEYWORDS: *quartz crystal microbalance, graphene, immunoassay, membranous nephropathy, biosensor*

Graphene-based materials are promising candidates for the development of drug delivery vectors and biosensors[1−5] due to their high specific surface area[6] and ease of functionalization.[7,8] The hydrophobicity of unmodified graphene materials and high sensitivity to charges and electrical fields, however, results in strong and nonspecific molecular adsorption, which leads to poor selectivity for biological analytes when operating in an aqueous environment.[9,10] The hydrophobic nature of graphene is known to denature proteins,[11] and the binding sites of protein receptors that are defined by their tertiary structures are disrupted, resulting in poor sensitivity and detection limit. Several methods have been reported to functionalize graphene-based materials with protein receptors[12−15] such that their tertiary structure and binding sites are preserved and presented. Noncovalent linkers, such as 1-pyrenebutanoic acid succinimide ester, *N*-hydroxysuccinimide (NHS) ester tripod, bovine serum albumin (BSA), and pyrene butyric acid (PBA), have been successfully used to construct a biointerface in graphene-based biosensors to detect glucose,[16] DNA,[14] proteins,[15,17] and other biomolecules.[18,19] Harnessing BSA as a biointerface layer offers various advantages including preventing non-specific binding,[17,20] improving biocompatibility,[21] ease of use,[22] and low cost.[17,22] Zhou *et al.* suggested a one-step method using thermally denatured BSA activated with EDC/NHS to construct a graphene field-effect transistor (GFET) for detecting a cancer biomarker, carcinoembryonic antigen.[22] However, FET biosensors suffer from lack of reproducibility of the signal when experimenting in concentrated biological samples like serum due to the high sensitivity to charges in the solutions.[23−25] Furthermore, the manufacturing complexities of graphene FETs remains a major challenge to mass-market adoption as a medical diagnostic device.[15,23,26]

We have developed a new biosensor instrument and technique based on a customized quartz-crystal microbalance (QCM), coupled with graphene biointerface sensing chips,[11,27] and demonstrate it as an immunoassay tool for detecting antibody biomarkers. QCM is a commonly used piezoelectric transducer for biosensing; it is a highly sensitive weighing device based on measuring the change in mechanical resonance of the quartz crystal corresponding to the change of mass adsorption according to Sauerbrey's equation.[28] This mechanism allows for sensitive, label-free, rapid detection of analytes and a reproducible response. Compared to QCM, other label-free transducers like surface plasmon resonance

Received: August 7, 2020
Accepted: October 13, 2020
Published: October 26, 2020

https://dx.doi.org/10.1021/acssensors.0c01641
ACS Sens. 2020, 5, 3520−3532

(SPR) sensors rely on optical detection of the molecules on the gold-coated sensor chip. SPR has become a global pharmaceutical and clinical research standard,[29] however, it requires expensive equipment and complex fabrication of sensors to accomplish high efficiency for biosensing compared to QCM transducers.[25,30,31] The most widely adopted method for the determination of immunochemical markers is enzyme-linked immunosorbent assay (ELISA), which is available as the first choice in most clinical laboratories. Due to its extremely high sensitivity, specificity, precision, and throughput, ELISA has served as the gold standard for various analytes.[32,33] The main challenges for ELISA assays include high cost, testing duration, and complexity owing to the many steps required to complete the assay[33] and the semiquantitative nature of the assay, which is based on a duplicate standard sample. For these reasons, specialized laboratories and highly skilled operators are required, resulting in the high costs of instrument and operation. With advantages of low cost, high sensitivity, rapid detection, and portable size, the QCM device described here shows promise as a point-of-care immunoassay tool, especially for remote locations or low and middle income (LMI) communities.

Nephrotic syndrome (NS) describes a constellation of symptoms that typically includes nephrotic range proteinuria, hypoalbuminemia, oedema with or without hyperlipidemia, and is caused by a number of different kidney diseases.[34−36] The syndrome is characterized by increased glomerular permeability.[34] Membranous nephropathy (MN) is a common cause of NS in adults. Primary membranous nephropathy (pMN) is found in 80% of MN patients affecting 10−12 cases per 1 million population.[37,38] The important discovery in 2009 that circulating antibodies to phospholipase A2 receptor (PLA2R) present in 70% of patients with pMN identified the autoimmune nature of this pathology.[39] As ∼80% of patients show proteinuria in the nephrotic range, they can be identified by the presence of edema on physical examination. However, this does not determine the type of nephrotic syndrome.[40] For this, a kidney biopsy is required and this will identify the histological features of MN. Additional time-consuming tests are then required to determine the specific autoantigen. Although pMN progresses slowly, and some patients can enter a spontaneous remission phase, 30−40% of patients eventually develop end-stage renal disease or die.[40−42]

Fresquet *et al.* identified variably sized constructs of PLA2R reacting with anti-PLA2R under denaturing conditions (western blotting) and non-denaturing conditions (native blotting).[35] They found that the dominant epitope of PLA2R was within the ricin-like N-terminal domain, which competed effectively for the binding of autoantibodies in approximately 90% of the tested patient sera, confirming the presence of a major epitope within the N-terminal fragment of the receptor. As a result, NC3, which is the N-terminal to CTLD3 fragment, was used as a receptor in this study.

We have previously demonstrated the development and use of graphene-coated (G-) QCM chips to study interactions between biomolecules and graphene surfaces.[11,27] We reported a simple method to obtain a film of denatured BSA (dBSA) on rGO.[11] By physical adsorption of BSA from a low-concentration solution in phosphate-buffered saline (PBS) onto highly hydrophobic rGO at room temperature, a denatured adlayer of BSA can be formed on the rGO. This method is a simple, fast, and cost-effective way to employ dBSA on graphene as an inert biointerface for immobilizing specific protein receptors in graphene biosensors.

In this work, we first use a commercial QCM with dissipation monitoring (QCM-D) system (QSense Pro, Biolin Scientific) to establish the immunosensing performance of the G-QCM chip by studying the binding interactions between the receptor NC3 and murine anti-PLA2R antibody (Ab12). With QCM-D measurements, the interaction dynamics between the receptor and analyte can be systematically investigated as the frequency parameter provides information about the mass adsorbed and film thickness, while the dissipation parameter can provide mechanical information such as viscoelasticity of the adsorbed film on underlying surfaces.[43,44]

One of the main disadvantages of the commercial QCM-D system for use as a point-of-care instrument is its high cost. This in turn leads to slow test times as samples will need to be sent to specialist laboratories. Here, we have developed a customized open-source-based QCM instrument where the openQCM system (Novaetech S.r.l., Italy) is the core sensing device,[45] hereafter referred to as the C-QCM. In contrast to the QSense system, in which low fundamental frequency crystals (5 MHz) are used in a flowing fluid, our C-QCM employs crystals with a fundamental frequency of 10 MHz in a static fluid configuration, which provides higher sensitivity. Both systems were used to quantify the antibody in buffer solutions and patient sera samples. The results obtained from patient sera measured by both systems were compared with each other and validated against results from ELISA tests. We demonstrate that our C-QCM instrument coupled with G-QCM crystals is capable of highly sensitive, quantitative, and reproducible immunoassay measurements in buffer and human serum, making it suitable for biological research, therapeutics development, as well as point-of-care clinical diagnostics.

MATERIALS AND METHODS

Materials and Reagents. GO dispersion was prepared by a modified Hummers' method[46] followed by exfoliation and purification. Briefly, graphite flakes of 50 mesh (1 g) and $NaNO_3$ (0.9 g) were mixed in concentrated H_2SO_4 (35 mL) and left overnight to intercalate. The mixture was cooled down in an ice bath before slowly adding 4.5 g of $KMnO_4$ while continuously stirring. The mixture was left for 5 days at room temperature to allow graphitic oxidation. The brown slurry was diluted by slowly adding 5% H_2SO_4 solution (100 mL) and then diluted again with a 100 mL mixture of 3% H_2SO_4 and 0.5% H_2O_2. The homogenization and complete exfoliation of graphite oxide were carried out using a vertical stirrer at a low speed for ∼1 h. The final GO dispersion was washed by repeated centrifugation and dilution with diluted H_2SO_4 followed by DI water, until the pH was close to neutral.

Albumin, monomer bovine (A1900), and phosphate-buffered solution (PBS, 0.1 M), pH 7.4 (P5244) (Sigma-Aldrich, UK) were used as received. BSA stock solution was prepared with a concentration of 1 mg/mL. The dilutions of BSA solution were prepared from the stock solution. The EDC and sulfo-NHS cross-linkers were purchased from Sigma-Aldrich (UK). Ethanolamine was used as a blocking buffer purchased from Sigma-Aldrich (UK). Bovine calf serum was purchased from Sigma-Aldrich (UK). The production of NC3 receptor was previously described by Fresquet *et al.*[35] The codon-optimized clone of human extracellular PLA2R was modified to generate the smaller PLA2R NC3 (∼90 kDa) fragment. NC3 stock solution was prepared with a concentration of 2.5 mg/mL in PBS. The stock solution was diluted in PBS to 25 μg/mL for using in all experiments. More details about the process of production are in Supporting Information Section 1. Murine anti-PLA2R monoclonal antibodies (Ab12) were generated previously for a binding study and determination of detection limit made in-house based on the protocol

https://dx.doi.org/10.1021/acssensors.0c01641
ACS Sens. 2020, 5, 3520−3532

from Mauchauffé *et al.*[47] The patient sera samples were from patients across the Northwest region of the UK who involved in the PRISM trial[48] carried out at the Manchester Institute of Nephrology and Transplantation, Manchester Royal Infirmary.

Customized openQCM Construction. The C-QCM system consists of an Arduino Micro microcontroller board and an electronic shield that holds the excitation circuit for the crystal (Pierce oscillator) and a digital temperature sensor (MCP9808) placed in close proximity to the quartz crystal. The crystal is supported by a HC-48U type quartz holder. An enclosure for the C-QCM device and a fluidic cell were custom designed and fabricated using a Formlabs Form 2 3D printer with clear resin (RS-F2-GPCL-04). The fluidic cell was designed to be suitable for pipetting liquid into the cell, see Figure 1a. The volume of the fluidic cell is approximately 35 μL. The gold-coated quartz crystals with a fundamental frequency of 10 MHz (AT10-CUT) were purchased from Quartz Pro (Sweden). A custom graphic user interface (GUI) for data visualization and recording was developed in Matlab R2018a. A figure of the complete setup of this device is included in Supporting Information Section 2.

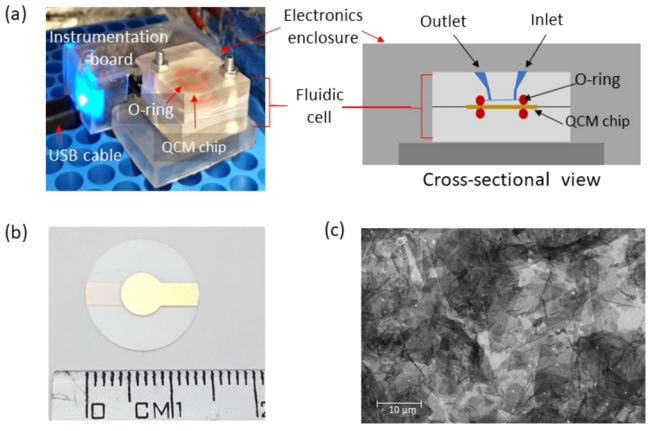

Figure 1. Photographs and layout of the sensor chip. (a) C-QCM instrument setup and cross-sectional schematic of the C-QCM device with a custom-designed microfluidic channel. (b) Photograph of an rGO-coated QCM sensing chip. (C) Scanning electron microscopy (SEM) image of the rGO coating on a QCM chip.

QCM Chip Surface Coating and Characterization. The stock dispersion of GO was diluted to a concentration of 0.8 mg/mL. QCM chips with a gold surface electrode for both QSense (QSX-301, Biolin Scientific) and the C-QCM (QCM10140CrAu051-051-C1, Quartz Pro) were used in this study. The chips were cleaned following the protocol provided in Meléndrez *et al.*[27] and then coated with GO via spin coating (speed: 3000 rpm, acceleration: 350 s^{-1}, 2 min) to form a GO film on the entire surface of the chip. A controlled thermal treatment of the GO-coated chips was performed in a vacuum oven (Townson+Mercer EV018) with a temperature of 180 °C for 6 h to reduce the GO and obtain a highly hydrophobic rGO coating as described in our previous study.[11]

The degree of reduction was characterized by means of their wetting contact angle (WCA) using sessile drops of DI water (Kruss DSA100) in combination with X-ray photoelectron spectroscopy (XPS) using a SPECS custom-built system composed of a Phobios150 hemispherical electron analyzer with 1D detector. The XPS data was analyzed using CasaXPS software (version 2.3.18). Scanning electron microscopy (SEM) was performed on a Zeiss Ultra using an accelerating voltage of 5 kV and 5 mm working distance with secondary electron imaging to characterize the morphology of graphene coatings on Au surfaces.

Receptor Immobilization and Antibody Binding Studies Using QCM-D. The NC3 receptor was immobilized on different functional surfaces followed by antibody-receptor binding studies under QCM-D monitoring using the QSense Pro system. The temperature of the system was stabilized at 25 °C to avoid the effects of thermal drift. The basic sequential injection steps for QCM-D monitoring of the antibody binding include the following: (1) a baseline stabilization regime in which PBS is flowed until stability is reached, (2) immobilization of the NC3 receptor, (3) blocking non-specific adsorption, and (4) detection of the antibody followed by rinsing. The complete procedure is described in Supporting Information Section 3.3. The concentrations of NC3 and the antibody in PBS were fixed at 25 and 1 μg/mL, respectively. In this work, the odd harmonics from the 3rd to the 11th were recorded. Our discussion of results is based on the 3rd harmonic. The measurement of the frequency shift after the adsorption of the antibody was used to investigate the capability of each sensing surface to detect the

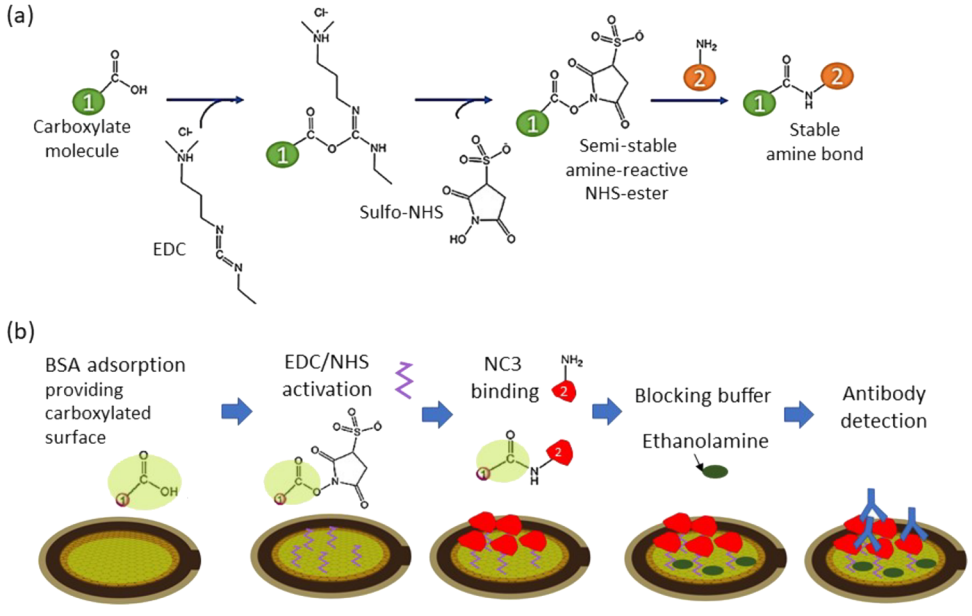

Figure 2. Schematic for surface functionalization using EDC/NHS cross-link: (a) mechanism of carbodiimide cross-linker using EDC/NHS activation and (b) functionalization of the rGO surface to detect the antibodies starting with BSA adsorption, amine activation with EDC/NHS, and immobilization of the receptor NC3 (in red) via amine covalent cross-link and blocking with ethanolamine.

https://dx.doi.org/10.1021/acssensors.0c01641
ACS Sens. 2020, 5, 3520−3532

antibody. From these observations, the highest shift was selected for further studies.

Concentration Sequence and Specificity Studies. Using the QCM-D system, the binding of various concentrations of Ab12 was first studied. The NC3 receptor at a concentration of 25 μg/mL in PBS was injected on the selected functional surfaces of the sensing chip following the receptor immobilization protocol (Supporting Information Section 3.3) followed by the injection of PBS to rinse the surface. Ethanolamine was used as a blocking agent to prevent non-specific adsorption on the amine functional groups.

Before binding with the antibody, the sensing surface was rinsed with PBS until baseline stability was reached and the acquisition was restarted. This procedure was repeated twice to ensure adequate cleanse of unbound molecules. Then, the diluted antibody was injected for approximately 20 min and finally rinsed with PBS for 20 min. The flow rate for this experiment was kept at 10 μL/min. Various concentrations of the antibody (0.5, 1, 20, 50, and 100 μg/mL) were monitored in this study where each sensing chip measured one concentration. A group of frequency shifts was recorded as a quantitative measure for each concentration of the antibody. The measurement for each concentration was repeated three times.

To evaluate the selectivity of the sensor in complex fluids such as serum, calf serum was used as a sample medium. Three different samples, namely, plain calf serum diluted with PBS 1:1 (negative control), 50 μg/mL Ab12 in the diluted calf serum, and 50 μg/mL Ab12 in PBS, were used in this experiment. QCM-D monitoring of adsorption of the samples on NC3-functionalized sensing chips were run at the same time to reduce variability due to environmental effects.

In addition, a QCM-D measurement was conducted in order to contrast the results of diluting various concentrations of the antibody in the diluted calf serum with those obtained from the series of the antibody concentration in PBS. The concentrations used for this experiment are 0.5, 1, 20, 50, and 100 μg/mL.

Ab12 Detection Using the C-QCM. The C-QCM system was then used to evaluate the detection of Ab12. The G-QCM sensing chips were functionalized with NC3 receptor using the same steps as for the QCM-D system, Figure 2c. In each step, 40 μL of the sample was pipetted into the fluidic cell and allowed to stabilize until the frequency signal was stable. This process was then followed by the injection of the next reagent. A peak in the frequency response occurs during the liquid injection due to the abrupt change of pressure on top of the sensing chip; however, the signal stabilizes within a few minutes. Due to the fact that QCM sensors with higher frequencies are prone to be affected by hydrodynamic pressure, a poor signal-to-noise ratio (SNR) is presented under flowing fluids, resulting in less sensitivity of the measurements.[49,50] Therefore, our measurements were performed under static fluid pressure in order to prevent any effects from eventual pump noise and to improve the sensitivity.

After functionalizing the receptor on the QCM chip and blocking the non-specific adsorption with the ethanolamine blocking buffer, the samples with different concentrations of the antibody in PBS buffer ranging from 0.1 to 100 μg/mL were assessed. For each measurement, the specimen was injected into the fluidic cell and allowed to bind for 10 min followed by the injection of PBS to rinse the surface until a flat signal was achieved, indicating that no further adsorption occurs. The final frequency shift was recorded as a value that corresponds to the antibody binding. This experimental procedure was repeated at least twice for each specimen.

Patient Serum Evaluation Using the QSense and the C-QCM. To investigate the feasibility of the C-QCM immunoassay for practical diagnostic applications, we analyzed eight human serum samples. Each serum sample was diluted with PBS to a ratio of 1:3. The QSense and the C-QCM systems were used to perform comparative analysis. The aforementioned procedures for the immobilization of the receptor and the measurement of antibody binding were applied. The testing protocol for the QSense system starts by flowing PBS over the functionalized chip for 5 min to obtain a baseline, and then the sample is injected with a flow rate of 10 μL/min for 20 min (total sample volume of 200 μL) and finally rinsed with PBS for at least 10 min. For the C-QCM system, the PBS solution was kept static over the functionalized QCM chip reading the settling frequency as a baseline and then 40 μL of the specimen was injected and let to be adsorbed for 10 min. After this, sequential injections of PBS were performed to rinse the surface of the chip until the observed signal was flat. Each test was repeated at least three times. The results from the two systems were compared to each other and with those obtained by the ELISA test performed in-house.

ELISA Assay. The ELISA tests were performed using serum samples from the patients across the Northwest region of the UK involved in the PRISM trial.[48] Samples were analyzed using our in-house ELISA using a previously published protocol.[51] The purified extracellular recombinant PLA2R protein was used to coat ELISA plates as a receptor for anti-PLA2R antibody. The plates were read at 450 nm, and standard curves were plotted using the Softmax software Molecular Devices (Sunnyvale, CA). A dilution series covering the range of 3000−12.3 U/mL was applied for each ELISA plate. The samples with ELISA results less than 40 U/mL were considered normal or negative. The upper limit is 3000 U/mL.

RESULTS AND DISCUSSION

Binding Studies. *Dot Blot.* The binding between the NC3 and the Ab12 was tested using the dot blot technique. A varied concentration set of NC3 and the denatured NC3 were used. The results and discussion from this evaluation are detailed in Supporting Information Section 4. In brief, it was confirmed that the Ab12 specifically binds with the non-denatured NC3.

Characterization of Graphene Coating and Functionalization. We have explored different methods to functionalize the protein receptor including both physical adsorption and covalent immobilization. Eight different functional surfaces were used in this comparative study, namely, (1) Au, (2) GO, (3) rGO, (4) Au with denatured BSA coating (Au-dBSA), (5) rGO with dBSA coating (rGO-dBSA), (6) rGO with non-denatured BSA coating (rGO-BSA), (7) Au with self-assembled monolayer (SAM) with COOH terminal groups (Au-SAM), and (8) rGO-dBSA activated with EDC/NHS for amine coupling (rGO-dBSA+EDC/NHS). Based on our previous paper, a denatured layer of BSA is formed when BSA is adsorbed on Au or highly hydrophobic rGO surface from a low concentration solution.[11]

SEM imaging reveals that the spun-on graphene coatings on the Au surface of QCM-D chips comprises a continuous film of overlapping flakes covering the entire surface, with film thickness varying from one to few monolayers (Figure 1c). The individual graphene flakes are composed of 100% of monolayers (Supporting Information Section 6). The graphene coverage is uniform over large areas on all samples studied (Supporting Information Section 6).

Surfaces with different stages of rGO functionalization were characterized using XPS and Raman. XPS spectra of rGO, rGO-dBSA, and rGO-dBSA-EDC/NHS were measured, see Figure S5 in Supporting Information Section 7. The C1s spectrum obtained from rGO displays a low intensity of oxygen functional groups but a high intensity of the carbon peak. Adsorbing BSA on rGO adds to the carboxylate groups. After activating rGO-BSA with EDC/NHS, the deconvoluted peaks of C−N and CO−NH were enhanced while C−O decreases. The spectrum for rGO-BSA cross-linking with EDC/NHS clearly shows the emergence of the C−N peak corresponding to the amine coupling on the denatured BSA on rGO, see the deconvoluted peaks in Figure S6. Further details about the XPS results are discussed in Supporting Information Section 7.

https://dx.doi.org/10.1021/acssensors.0c01641
ACS Sens. 2020, 5, 3520−3532

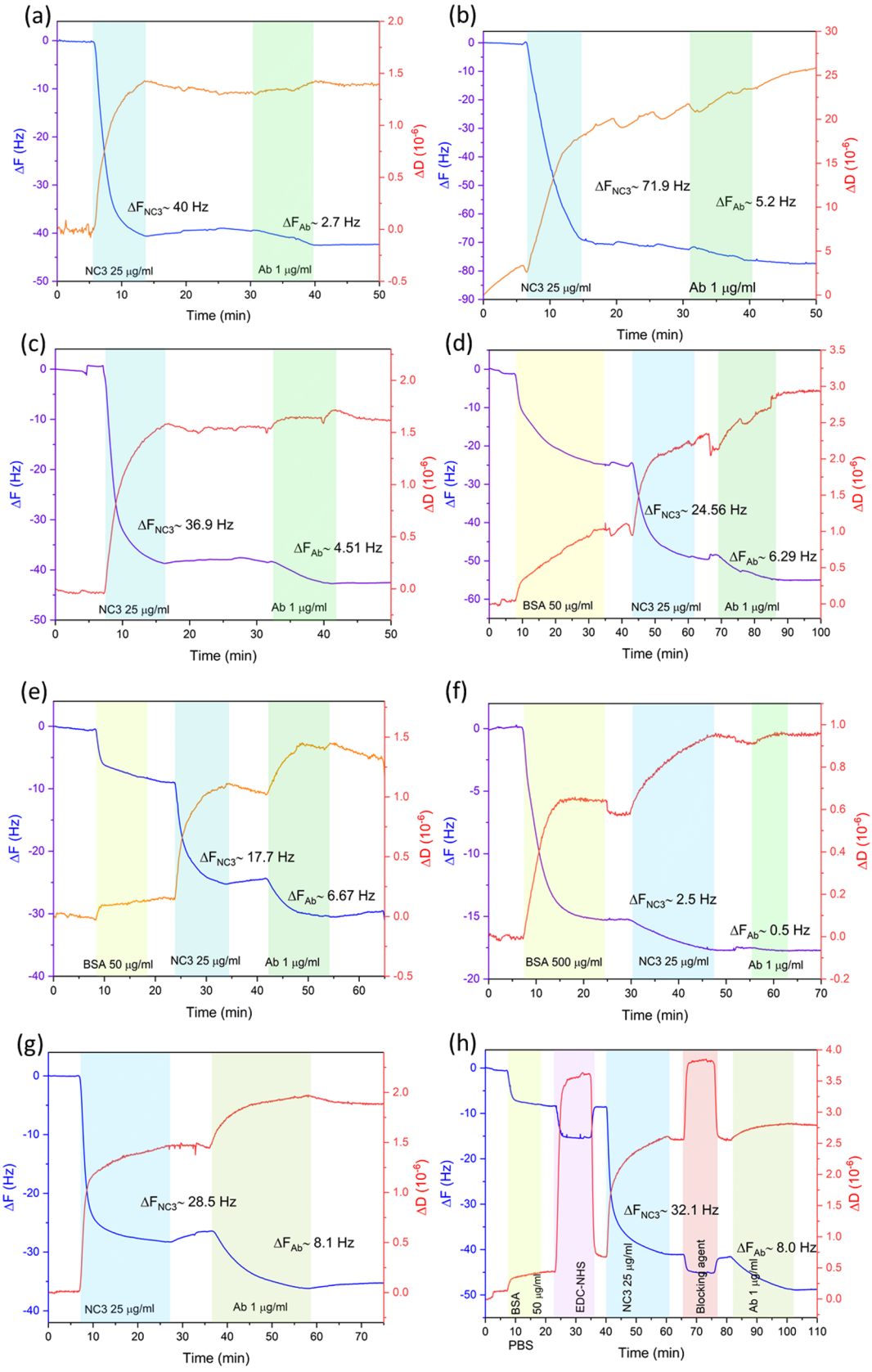

Figure 3. QCM-D monitoring of receptor protein (NC3) immobilization and anti-PLA2R antibody (Ab12) detection using different sensing surfaces: (a) Au, (b) GO, (c) rGO, (d) Au-dBSA, (e) rGO-dBSA, (f) rGO-BSA, (g) Au-SAM, and (h)rGO-dBSA+EDC/NHS.

Raman spectra of rGO, rGO-dBSA, and rGO-dBSA+EDC/NHS were measured to obtain information about lattice defects, see Supporting Information Section 8. Two main peaks, graphitic (G) and defect (D), occur at ~1580 and

https://dx.doi.org/10.1021/acssensors.0c01641
ACS Sens. 2020, 5, 3520−3532

Table 1. QCM-D Results of the Adsorption of NC3 (Receptor) and Ab12 (Analyte) on All Sensing Surfaces for Comparison of Sensing Performance

		NC3 (receptor)		Ab12 (analyte)	
sample no.	surfaces	ΔF (Hz)	ΔD ($\times 10^{-6}$)	ΔF (Hz)	ΔD ($\times 10^{-6}$)
1	Au	40.0 ± 0.8	1.39 ± 0.05	2.7 ± 0.8	0.08 ± 0.2
2	GO	70.0 ± 11.3	16.1 ± 4.5	5.4 ± 1.2	5.03 ± 2.3
3	rGO	36.0 ± 0.7	1.53 ± 0.02	4.5 ± 0.8	0.14 ± 0.05
4	Au-dBSA	24.6 ± 3.2	1.21 ± 0.08	6.5 ± 2.1	0.56 ± 0.08
5	rGO-dBSA	17.7 ± 1.1	0.89 ± 0.06	6.5 ± 1.3	0.33 ± 0.05
6	rGO-BSA	2.4 ± 0.8	0.37 ± 0.03	0.2 ± 0.1	0.03 ± 0.01
7	Au-SAM	27.0 ± 1.2	1.47 ± 0.04	8.0 ± 1.2	0.50 ± 0.2
8	rGO-dBSA+EDC/NHS	32.5 ± 4.3	1.89 ± 0.07	8.1 ± 2.2	0.40 ± 0.04

~1350 cm^{-1}, respectively. The relative intensity of D to G (I_D/I_G) indicates the in-plane crystallite size or the disorder in the sample. The I_D/I_G value of rGO is 0.89, which is lower than that of rGO-dBSA and rGO-dBSA+EDC/NHS samples, which exhibit similar I_D/I_G values of 0.97 and 0.95, respectively. The higher I_D/I_G values obtained from functionalized rGO samples could originate from defects and effects of doping functional groups through BSA adsorption. Two other bands were observed at 2700 and 2900 cm^{-1}, known as 2D and D+G peaks, respectively. The 2D band is an indicator of the number of graphene layers if it is a sharp peak. Another band is a second-order peak derived from the D−G peak combination. All samples present a broadened band, attributed to the fact that the graphene coating contains few layers with some defects from oxygen functional groups in rGO and protein doping.

Exploration of Sensing Surfaces Using QCM-D. The results from the QCM-D monitoring of the receptor protein (NC3) immobilization on different sensing surfaces and the detection of Ab12 are presented in Figure 3. The resultant frequency shifts from the adsorption of NC3 (receptor) and Ab12 (analyte) are given in Table 1.

The adsorption of NC3 on Au and rGO surfaces display lower dissipation values compared to GO possibly due to the different orientation of the molecules on the surfaces.[11] When high dissipation values were obtained, higher errors on the frequency shifts occurred as it can be observed in Table 1. Thus, we propose that the GO surface is not suitable to be used as a sensing platform for a traditional QCM immunoassay as it could result in high detection errors. Direct immobilization of NC3 on Au and rGO detected less antibody compared to those surfaces with an adlayer of BSA (samples 4 and 5) as the thin layer of BSA could prevent the denaturation of the NC3 during the adsorption process.[11] However, the rGO with non-denatured BSA sensor (sample 6) presents relatively less adsorption of NC3 and no binding of the Ab12 was detected. This is due to the fact that BSA acts as a blocking agent, preventing other molecules to adsorb onto the surface.

Quantitatively, the detection of antibody was higher on the platform using the covalent binding methods (samples 7 and 8) as specific-binding sites can be promoted through the cross-link of functional groups. Both the rGO-dBSA+ EDC/NHS and the Au-SAM samples present the highest antibody binding responses, in terms of the frequency shifts, with similar values of approximately 8.0 Hz. We reason that the covalent binding due to amine coupling on the carboxylate surface can promote the specific-site binding of NC3 on the surface and reduce its denaturation, allowing the antibody biding sites to remain actively functional. The mechanism of EDC/NHS activation is presented in Figure 2a.

Although both surfaces present comparable results for antibody detection, the preparation of the rGO-BSA+EDC/NHS surface requires simple adsorption of the protein and an activating agent on rGO at room temperature, a process that is much simpler and less time-consuming compared to Au-SAM preparation requiring more chemicals and overnight preparation (see Supporting Information Section 5 for details of Au-SAM preparation). Therefore, the rGO-BSA+EDC/NHS platform was selected for further studies.

Ab12 Detection and Specificity Analysis Using QCM-D. The rGO-dBSA+EDC/NHS surface was used as a sensing platform for this study. The schematic for QCM surface functionalization using EDC/NHS cross-link is presented in Figure 3 with the following injection sequence: BSA 50 μg/mL → EDC/NHS → NC3 → blocking buffer → antibody sample. We observe that both the frequency and dissipation increase as a function of the antibody concentration. The adsorption rate increases with respect to the concentrations. After the rinsing step, some loosely bound molecules lifted off from the surface as observed from the decrease of the frequency shift.

The detection of Ab12 with the NC3, at various concentrations ranging from 0.5 to 100 μg/mL in PBS, was monitored in real time using the QCM-D technique (Figure 4a). The frequency shift (ΔF) obtained from the QCM-D measurement relates to the mass adsorbed on the sensing surface, while the dissipation change (ΔD) is related to the viscosity of the adsorbed material. Further details on the QCM-D operation principle are discussed in Supporting Information Section 3. From the $\Delta D-\Delta F$ plot of the QCM-D results (Figure 4b), the slope increases with respect to the concentration of the antibody.

The results of the selectivity test with calf serum are presented in Supporting Information Section 9. The adsorption of three different samples, (1) the negative control calf serum, (2) 50 μg/mL Ab12 in the diluted calf serum, and (3) 50 μg/mL Ab12 in PBS, on NC3-functionalized sensing chips were obtained at the same time and under the same environmental conditions. Sample (1) exhibits a final frequency shift of ~8 Hz, which corresponds to the serum background, while sample (2) presents a final shift of ~24 Hz. By subtracting the frequency shift in sample (1) from sample (2), the result is similar in value to that from sample (3). These results confirm that the binding of the antibody can be selectively detected directly in concentrated animal serum. The concentration of antibody in serum can be quantified by subtracting the final frequency shift from the background value obtained from the plain serum.

https://dx.doi.org/10.1021/acssensors.0c01641
ACS Sens. 2020, 5, 3520−3532

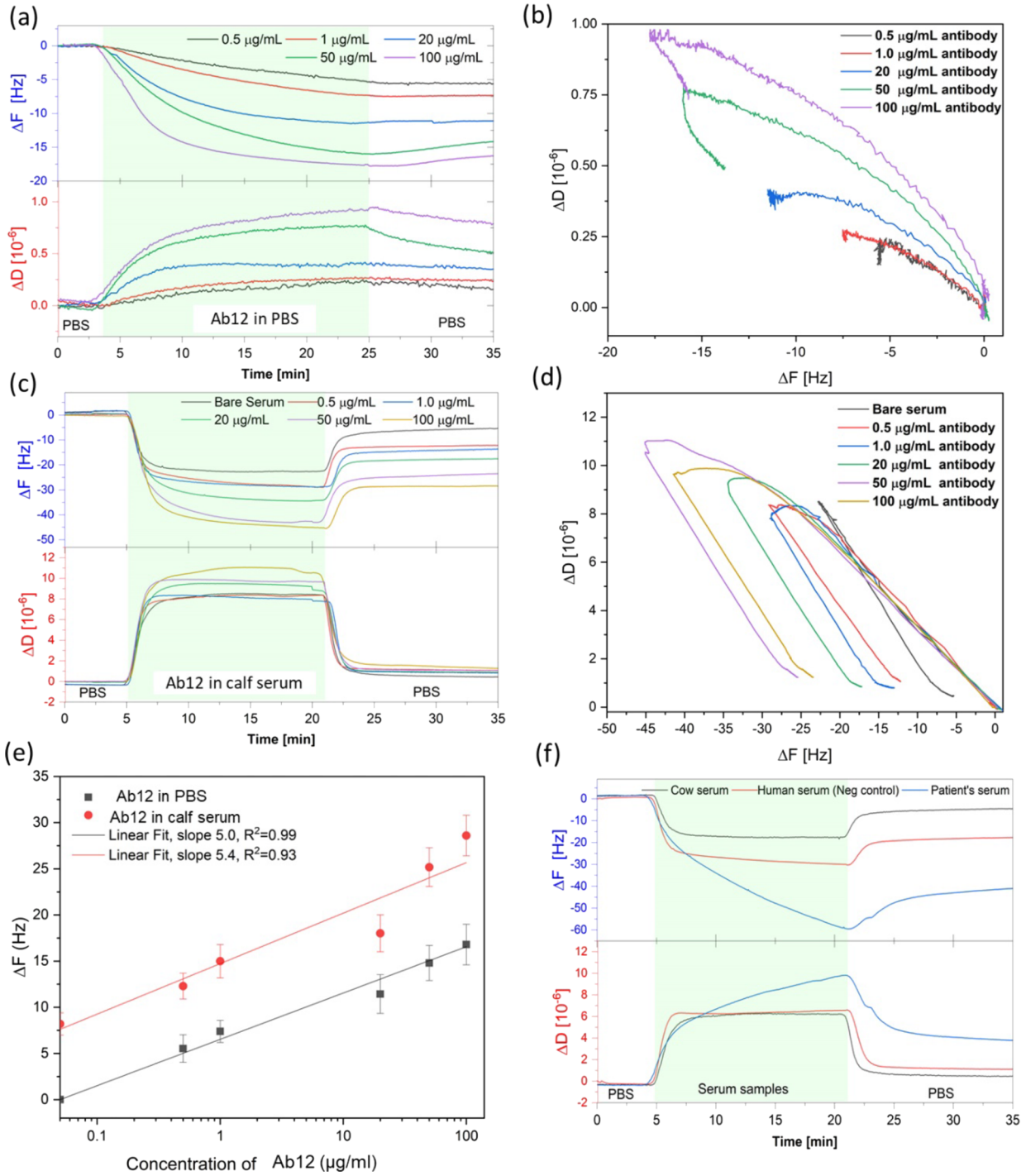

Figure 4. QCM-D results for binding studies: (a) frequency and dissipation profiles upon detection of varied concentrations of the Ab12 in PBS buffer and (b) their $\Delta D-\Delta F$ plots of the antibody detection. (c) QCM-D monitoring of varied concentrations of the Ab12 in calf serum and (d) their $\Delta D-\Delta F$ plots. (e) Comparison of the detection results obtained from varied concentration of the antibody in PBS and calf serum. (f) QCM-D monitoring of three serum samples: plain calf serum, human sera from a healthy person, and a MN patient.

The binding of various concentrations of the Ab12 in calf serum (ranging from 0.5 to 100 μg/mL) was measured, shown in Figure 4c. During the adsorption process (green band), all samples exhibited the same high adsorption rate at the initial stage. In addition, the $\Delta D-\Delta F$ plot (Figure 4d) shows that the initial slopes are of the same value, implying that the same adsorption event occurs. Thus, we reason that this adsorption behavior could result from loading the serum on the chips.

Then, the adsorption rate for each sample slows down or flattens due to a possible saturation of the surface. After the rinsing step, the final frequency for each sample shifted back by approximately 25 Hz as non-specific and unbound molecules in the serum were rinsed off. However, the final energy dissipation values observed from all concentrations are similar, between 0.5 and 1.3 $\times$ 10^{-6}. Interestingly, in the case of blank serum, the $\Delta D-\Delta F$ graph shifts back immediately after reaching the highest point while the other cases exhibit

https://dx.doi.org/10.1021/acssensors.0c01641
ACS Sens. 2020, 5, 3520−3532

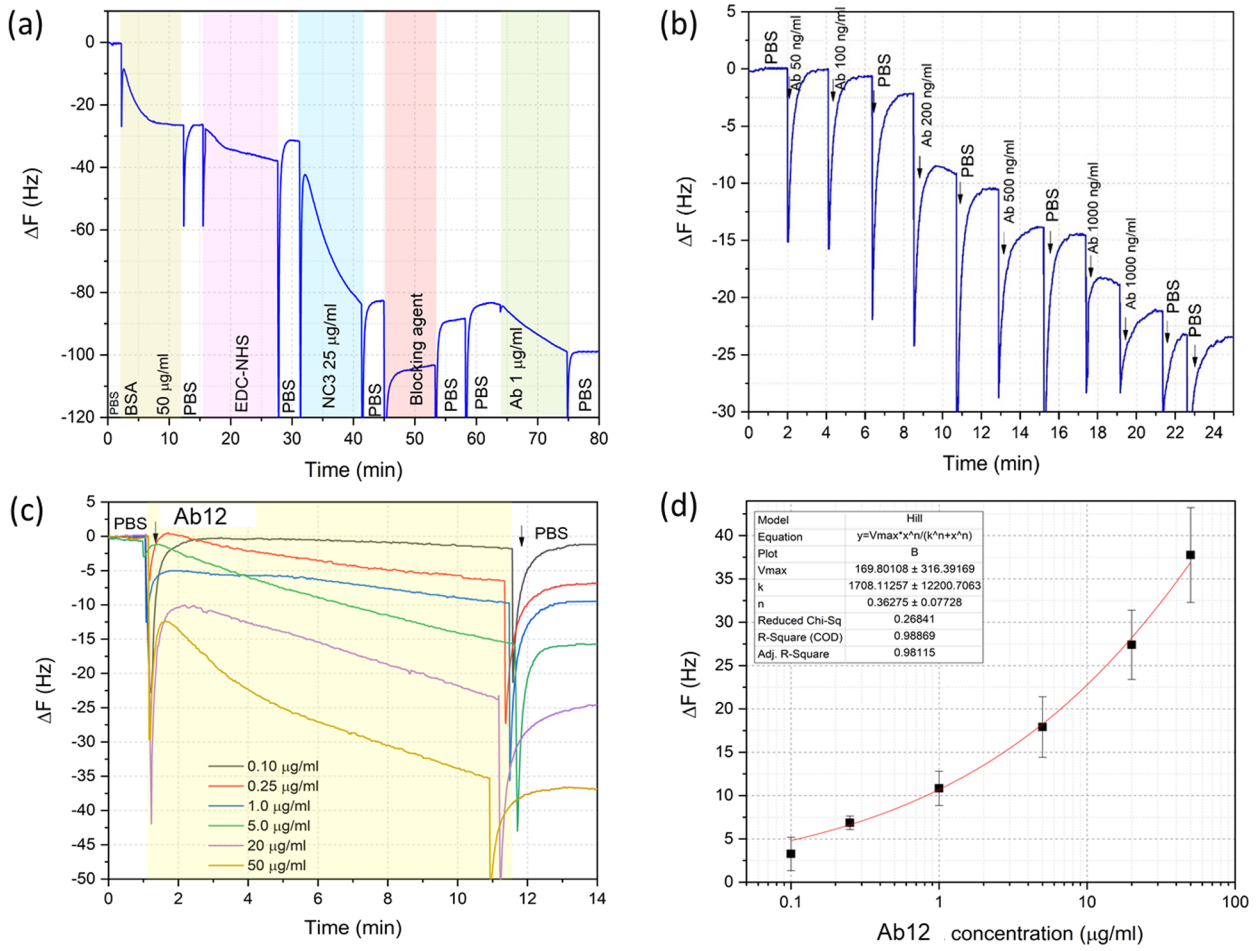

Figure 5. Results from Ab12 antibody detection using C-QCM system. (a) The whole injection sequence, (b) QCM results for sequential injection of varied concentrations of the Ab12 samples, (c) QCM profile for varied concentrations, and (d) calibration curve obtained from the final frequency shifts against the concentration of the antibody.

association curves at the highest region (Figure 4d). We assume that the association curves could originate from the antibody binding.

Figure 4e shows the comparison between the detection of the antibody in PBS and in calf serum by plotting the Ab12 concentration against frequency shift. A series of frequency shifts obtained from the antibody in calf serum are higher than those in PBS around 8 Hz due to the serum background. However, the plots from both series show similar trends with slopes of 5.0 and 5.4 for the antibody in PBS and in calf serum, respectively. Therefore, the frequency shift can be used as a comparative value to indicate the antibody concentration.

Figure 4f presents the comparison of the antibody detection in three different media, namely, plain calf serum, human serum from a healthy person (blank), and MN-patient serum (serum with high anti-PLA2R). The final frequency shifts obtained from these three samples are 8.5, 20, and 44 Hz, respectively. As the adsorption results from blank human serum are higher than that from calf serum, it suggests that non-specific binding in the assay is higher in human serum than in calf serum.

Detection of Ab12 Using the C-QCM System. Before the immunoassay studies, our C-QCM system setup and rGO-coated chips were tested for reproducibility when liquid samples were sequentially injected via pipetting. DI water and PBS buffer were used as liquid samples. The results are presented in Supporting Information Section 11. The resultant frequency shifts due to the weight of DI and PBS buffer are 2107 and 2361 Hz with standard deviations of 18 and 19 Hz, respectively. The observed values are in line with the results presented by Kanazawa and Gordon for the air−water loading of QCM sensors.[52,53] We conclude that the measurements using this C-QCM system could display an error of up to 1%, reflecting good reproducibility of the proposed technique.

To detect the Ab12 using the C-QCM, we replicated the same analytical steps from the QCM-D experiments including the doping BSA on rGO, the activation using EDC/NHS, receptor immobilization, and blocking, as shown in Figure 5a. The overall frequency monitoring from both QSense and C-QCM systems presents similar responses.

We further investigated the quantitative analysis capabilities of this immunoassay system with a series of antibody concentrations in PBS samples. We initially explored the detection in one QCM chip, see Figure 5b. The antibody concentrations, ranging from 0.05 to 50 μg/mL, were injected on to the functionalized chip. An observable frequency change occurs when the antibody concentration is equal or higher than 0.1 μg/mL. After the initial exploration, we detected the level of antibody binding from individual concentrations. The final ΔF value was recorded after 10 min from the initial injection of the sample followed by rinsing with PBS. The measurements were repeated at least three times. Figure 5a,b presents the

https://dx.doi.org/10.1021/acssensors.0c01641
ACS Sens. 2020, 5, 3520−3532

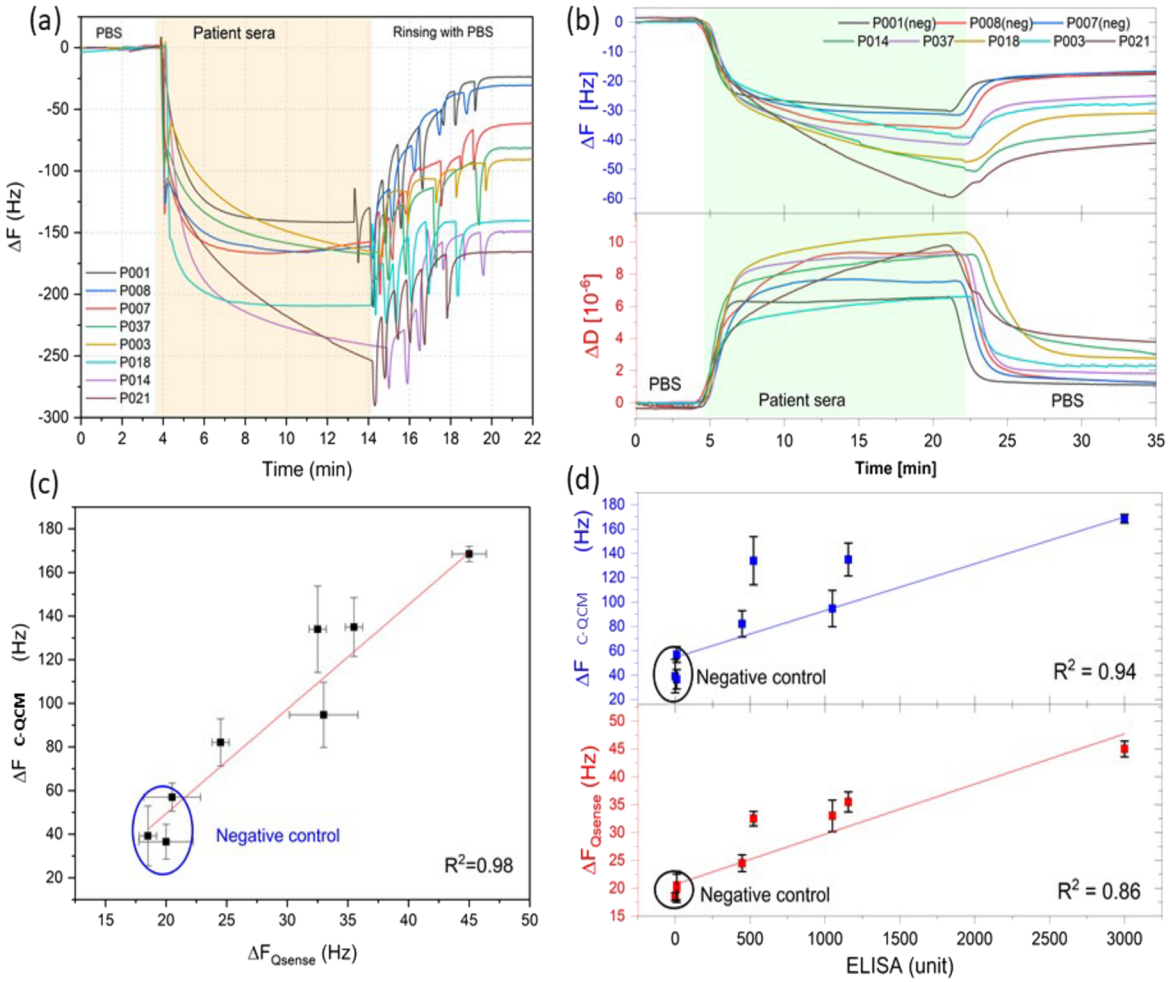

Figure 6. Detection results for the anti-PLA2R antibody in eight patients' sera using (a) the C-QCM system and (b) QCM-D system. (c) Correlation plot of the final frequency shifts obtained from the C-QCM and the QCM-D. (d) Comparison of the results obtained from C-QCM measurements and ELISA.

QCM profiles for the different antibody concentrations and the plot of the final ΔF value for each concentration. It is clear that the ΔF value linearly increases with respect to the antibody concentration. In these two experiments, the detection limit was estimated to be 100 ng/mL. The obtained mean ΔF for 0.10 μg/mL is 4.1 $\pm$ 1.7 Hz.

Previous reports have suggested that the cutoff point for an abnormal anti-PLA2R-IgG concentration can be defined as >0.9 μg/mL.[34,54] Huang *et al.* quantified the anti-PLA2R-IgG antibody concentration in 45 healthy volunteers, 31 IgA nephropathy, 9 lupus nephropathy, and 52 pMN patients using a fluorescence-based immunoassay.[34] They reported that serum anti-PLA2R-IgG levels in healthy volunteers ranged from 0.09 to 0.91 μg/mL.[54] Based on this cutoff concentration, the developed QCM immunoassay can detect the concentration of anti-PLA2R antibody at about one magnitude lower than the cutoff value.

Comparison between QCM-D and the C-QCM. Comparing the results obtained using the QSense and the C-QCM, certain similarities and differences were observed. Considering all the steps involved in performing an immunoassay using the QCM-D and the C-QCM instruments, as seen in Figure 2h and Figure 5a, the sequential frequency shifts and recoveries recorded by both systems look similar. However, there are specific differences between the results from the two systems due to the use of different crystals and measuring protocols.

First, frequency spikes occurred at the injection points in the result from the C-QCM due to the change of hydrodynamic pressure during pipetting. However, it does not affect the overall measurement if the signal is allowed to stabilize.

Second, the frequency shift values for each injection step monitored by the C-QCM are higher than the values from the QSense because higher fundamental frequency crystals (10 MHz) were used in a static fluid configuration in the C-QCM, while 5 MHz crystals were used in the QSense under fluid flow. With the same amount of adsorption, in theory, the frequency shift value obtained from the 10 MHz crystal should be four times higher the 5 MHz one. However, the main problem of using high fundamental frequency crystal is a low signal-to-noise ratio,[49] especially in liquid-phase adsorption as the signal can be really fluctuated due to unstable liquid flow, and the full 4x gain is not achieved. Third, the total assay time spent on the C-QCM is less than the total time for the QCM-D measurement. As 10 MHz crystals were used, higher ΔF results are presented in a shorter time. The ΔF results for the detection of 1 μg/mL Ab12 in PBS obtained from the QSense and the C-QCM are ~7 and ~18 Hz, respectively. The clear change of ΔF for antibody detection can be seen in 10 min when using the C-QCM.

https://dx.doi.org/10.1021/acssensors.0c01641
ACS Sens. 2020, 5, 3520−3532

Table 2. Comparison of Existing Techniques for the Anti-PLA2R Detection

technique	label	detection limit lower (ng/mL)	detection limit upper (ng/mL)	sample	assay time (hr)	cost (per instrument or test kit)	ref.
commercial ELISA	yes	0.6	10	buffer or diluted serum 1:100	3.5	inst.: £50k test: £30	55
fluoroimmunoassay	yes	30	3400	buffer or diluted serum 1:100	3.5	inst.: £50k test: £300	34
SPR	no	100	>3000	buffer	1	inst.: £200k test: £400	36
QCM-D (QSense, 5 MHz crystal)	no	500	10^5 (100 μg/mL)	buffer or concentrated serum	1	inst.: £40−£100k test kit: £200−£400	this work,[56]
C-QCM (10 MHz crystal)	no	100	10^5 (100 μg/mL)	buffer or concentrated serum	0.5	inst.: £1000 test kit: £20	this work

Testing with Patient Serum Samples. To validate the feasibility of developing the QCM immunoassay for clinical applications, we analyzed eight human serum samples obtained from patients living in the UK using the commercial QCM-D from QSense and our C-QCM system and compared our results with those obtained by ELISA.

Figure 6a presents the QCM profiles measured by the C-QCM system. Samples P001, P007, and P008 are negative controls. The final ΔF values range from 30 to 170 Hz. Figure 6b displays the frequency and dissipation changes after testing with patient sera obtained from the QCM-D measurement. The final ΔF values are in the range of 20−50 Hz, and ΔD values after rinsing are between 1.7×10^{-6} and 4.5×10^{-6}. The final ΔD value linearly corresponds to the final ΔF for each specimen, shown in Supporting Information Section 12. Yet, ΔD profiles during serum adsorption present a different trend to the final values resulting from the differences in viscosity of patient sera. By comparing the ΔF results obtained from the QSense and the C-QCM, we obtained the regression equation $y = 4.8(\pm 0.2)x - 46(\pm 9)$, where x represents the frequencies for the QSense system while y corresponds to the frequencies for our C-QCM. A correlation coefficient (R^2) of 0.98 was obtained, shown in Figure 6c. This indicates that the results from both systems are comparable in terms of quantitative analysis and specificity.

We compared QCM results obtained from both systems to those obtained from ELISA, which is a standard immunoassay method to screen patients. As can be seen in Figure 6d, ΔF results from both QCM systems show correlated results to those from ELISA titration with R^2 values of 0.94 for the C-QCM and 0.86 for the QSense. Moreover, specimens with very low or zero anti-PLA2R (negative control) can be identified using the C-QCM and present consistency to the ELISA results. These results indicate that the C-QCM immunoassay could be comparable to ELISA in terms of analytical sensitivity, thus providing an alternative tool for rapid clinical diagnosis, particularly for the screening of membranous nephropathy.

Comparison with Other Techniques. In the C-QCM, higher fundamental frequency QCM chips (10 MHz) were used to achieve higher sensitivity compared to QSense. As can be seen in Table 2, the C-QCM offers lower detection limit to the antibody binding compared to the QSense system. This also results in a less amount of serum sample (40 μL for the C-QCM and 200 μL for the QSense) required for the test.

Comparing with SPR, which is a commonly used label-free technique, the QCM system presents a similar detection limit of the anti-PLA2R to the SPR.[35,36] Fresquet *et al.* used the SPR to study the binding of the anti-PLA2R antibody on immobilized NC3 and other PLA2R domains. The detection limit of the antibody concentration was shown to be 1 nM (~100 ng/mL).[35] Another advantage of the QCM over the SPR is that the QCM can be used with concentrated to whole serum or viscous specimens while the sample for the SPR needed to be highly diluted or in buffer. Thus, a specialized laboratory with professional technicians is required to perform the test. These drawbacks also apply for ELISA and other optical sensing techniques, although the sensitivity obtained from those techniques could be higher. Additionally, the C-QCM is a rapid assay that can be completed within 30 minutes, whereas ELISA requires a few hours to complete plus the additional control sample. Testing time is important for disease screening as it can speed up clinical diagnosis. Another significant advantage of the C-QCM assay over other techniques is the low cost of testing kits and the instrument. As the C-QCM is an electronic-based and label-free sensor, expensive elements like optical systems and label chemicals or antibodies are not required. For these reasons, the C-QCM system can potentially be developed as a point-of-care clinical diagnosis tool.

CONCLUSIONS

We have shown that rGO coating on QCM chips helps improve surface functionality as it allows hydrophobic interactions and $\pi-\pi$ stacking to bind with biomolecules; however, it could denature the protein due to the strong hydrophobic nature of the interaction. We proposed to use a dBSA layer formed on the graphene surface of G-QCM chips to serve as an inert layer and a biofunctional cross-linker to conjugate the protein receptor NC3 to detect the anti-PLA2R antibody, the biomarker for diagnosis of membranous nephropathy (MN). QCM-D results verified that the dBSA layer acted both as a blocking layer against non-specific interactions from complex fluids while also maintaining the NC3 protein in a suitable conformation for ligand binding. We have shown that functionalizing hydrophobic two-dimensional (2D) materials using dBSA could offer controllable functionalization methods for various biointerfaces for immunosensors, nanomedicine, and drug delivery.

As the QCM-D system from QSense exhibits inadequate sensitivity for the antibody detection, as well as possessing other disadvantages such as high cost and complexity of operation, we have developed our C-QCM system to overcome these limitations. The proposed assay enables quantitative detection of the anti-PLA2R concentrations as

https://dx.doi.org/10.1021/acssensors.0c01641
ACS Sens. 2020, 5, 3520−3532

low as 0.1 μg/mL, which is a magnitude lower than the cutoff concentration for patients with MN. Our results for human serum specimens from healthy people and patients demonstrate that the detection sensitivity and specificity of the QCM immunoassay are comparable to those of ELISA. Moreover, the C-QCM offers advantages over the conventional methods in that the analytical operations are more rapid, easier to perform, no sample pre-treatment required, and less expensive. Our C-QCM method with G-QCM chips can be tailored as an on-field applicable tool for rapid clinical diagnosis and screening in remote areas or epidemic situations. More importantly, this technology could be extended to other autoimmune tests for wider diagnostic applications.

DECLARATION

This study has full ethical approval by the NHS Health Research Authority Research Ethics Committee (REC reference 16/NW/0560). All study sites also have local Research and Development approval. All samples obtained under the auspices of the Manchester Renal Biobank 2016–2021 and the PRISM trial.[48] All patients provided written informed consent, and the studies had full ethical approval from the NHS Health Research Authority Research Ethics Committee (PRISM - REC reference 16/NW/0560; Manchester Renal Biobank 2016–2012 - REC reference 16/NW/0119), along with local Research and Development approval.

ASSOCIATED CONTENT

Supporting Information

The Supporting Information is available free of charge at https://pubs.acs.org/doi/10.1021/acssensors.0c01641.

Information on the production of the receptor NC3; a discussion on the principle of CQM-D; the protocols for QCM measurement using both the QSense system and our customized QCM instrument; dot blot results; and characterization data on the graphene materials including SEM, XPS, and Raman spectroscopy; selectivity testing results, desorption study results; and results from patient sera studies (PDF)

AUTHOR INFORMATION

Corresponding Author

Aravind Vijayaraghavan − *Department of Materials and National Graphene Institute, Faculty of Science and Engineering, The University of Manchester, Manchester M13 9PL, U.K.*; orcid.org/0000-0001-8289-2337; Email: aravind@manchester.ac.uk

Authors

Piramon Hampitak − *Department of Materials and National Graphene Institute, Faculty of Science and Engineering, The University of Manchester, Manchester M13 9PL, U.K.*

Thomas A. Jowitt − *School of Biological Sciences, Faculty of Biology Medicine and Health, The University of Manchester, Manchester M13 9PL, U.K.*

Daniel Melendrez − *Department of Materials and National Graphene Institute, Faculty of Science and Engineering, The University of Manchester, Manchester M13 9PL, U.K.*

Maryline Fresquet − *School of Biological Sciences, Faculty of Biology Medicine and Health, The University of Manchester, Manchester M13 9PL, U.K.*

Patrick Hamilton − *Wellcome Centre for Cell-Matrix Research, Division of Cell-Matrix Biology and Regenerative Medicine, School of Biological Sciences, Faculty of Biology Medicine and Health, The University of Manchester, Manchester Academic Health Science Centre, Manchester M13 9PT, U.K.; Manchester Academic Health Science Centre (MAHSC), The University of Manchester, Manchester M13 9PL, U.K.*

Maria Iliut − *Department of Materials and National Graphene Institute, Faculty of Science and Engineering, The University of Manchester, Manchester M13 9PL, U.K.*

Kaiwen Nie − *Department of Materials and National Graphene Institute, Faculty of Science and Engineering, The University of Manchester, Manchester M13 9PL, U.K.*

Ben Spencer − *Department of Materials and National Graphene Institute, Faculty of Science and Engineering, The University of Manchester, Manchester M13 9PL, U.K.*; orcid.org/0000-0002-1453-5327

Rachel Lennon − *Wellcome Centre for Cell-Matrix Research, Division of Cell-Matrix Biology and Regenerative Medicine, School of Biological Sciences, Faculty of Biology Medicine and Health, The University of Manchester, Manchester Academic Health Science Centre, Manchester M13 9PT, U.K.; Department of Paediatric Nephrology, Royal Manchester Children's Hospital, Manchester University Hospitals NHS Foundation Trust, Manchester Academic Health Science Centre, Manchester M13 9WL, U.K.*

Complete contact information is available at: https://pubs.acs.org/10.1021/acssensors.0c01641

Notes

The authors declare no competing financial interest.

ACKNOWLEDGMENTS

P.H. acknowledges the financial support of the Development and Promotion of Science and Technology Talents Project (DPST), Thailand. D.M. acknowledges The National Council for Science and Technology (CONACyT), Mexico for the financial support. A.V. acknowledges the Engineering and Physical Sciences Research Council (EPSRC) grant EP/L01548X/1. We acknowledge the support of the Biomolecular analysis facilities, Faculty of Biology Medicine and Health, The University of Manchester. This work was supported by a Wellcome Trust Senior Fellowship award (202860/Z/16/Z) to R.L. The authors also acknowledge core funding from the Wellcome Trust (203128/Z/16/Z) to the Wellcome Centre for Cell-Matrix Research at the University of Manchester.

REFERENCES

(1) Vilhena, J. G.; Rubio-Pereda, P.; Vellosillo, P.; Serena, P. A.; Pérez, R. Albumin (BSA) Adsorption over Graphene in Aqueous Environment: Influence of Orientation, Adsorption Protocol, and Solvent Treatment. *Langmuir* **2016**, *32*, 1742–1755.

(2) Chung, C.; Kim, Y.-K.; Shin, D.; Ryoo, S.-R.; Hong, B. H.; Min, D.-H. Biomedical Applications of Graphene and Graphene Oxide. *Acc. Chem. Res.* **2013**, *46*, 2211–2224.

(3) Suvarnaphaet, P.; Pechprasarn, S. Graphene-based materials for biosensors: A review. *Sensors* **2017**, *17*, 2161.

(4) Mas-Moruno, C., *Surface functionalization of biomaterials for bone tissue regeneration and repair*; Elsevier Ltd.: 2018.

(5) McCallion, C.; Burthem, J.; Rees-Unwin, K.; Golovanov, A.; Pluen, A. Graphene in therapeutics delivery: Problems, solutions and future opportunities. *Eur. J. Pharm. Biopharm.* **2016**, *104*, 235–250.

(6) Geim, A. K.; Novoselov, K. S. The rise of graphene. *Nat. Mater.* **2007**, *6*, 183–191.

(7) Hirtz, M.; Oikonomou, A.; Georgiou, T.; Fuchs, H.; Vijayaraghavan, A. "Multiplexed biomimetic lipid membranes on graphene by dip-pen nanolithography," no. May, 2013, *4*, 2591, DOI: 10.1038/ncomms3591.
(8) Wang, Y.; Li, Z.; Wang, J.; Li, J.; Lin, Y. Graphene and graphene oxide: Biofunctionalization and applications in biotechnology. *Trends Biotechnol.* **2011**, *29*, 205−212.
(9) Sarmento, B.; das Neves, J., *Biomedical applications of functionalized nanomaterials : concepts, development and clinical translation*; Elsevier: 2018.
(10) Capomaccio, R.; Ojea Jimenez, I.; Colpo, P.; Gilliland, D.; Ceccone, G.; Rossi, F.; Calzolai, L. Determination of the structure and morphology of gold nanoparticle−HSA protein complexes. *Nanoscale* **2015**, *7*, 17653−17657.
(11) Hampitak, P.; Melendrez, D.; Iliut, M.; Fresquet, M.; Parsons, N.; Spencer, B.; Jowitt, T. A.; Vijayaraghavan, A. Protein interactions and conformations on graphene-based materials mapped using quartz-crystal microbalance with dissipation monitoring (QCM-D). *Carbon* **2020**, *165*, 317−327.
(12) Georgakilas, V.; Tiwari, J. N.; Kemp, K. C.; Perman, J. A.; Bourlinos, A. B.; Kim, K. S.; Zboril, R. Noncovalent Functionalization of Graphene and Graphene Oxide for Energy Materials, Biosensing, Catalytic, and Biomedical Applications. *Chem. Rev.* **2016**, *116*, 5464−5519.
(13) Lin, C.; Zhao, M.; Xi, G.; Wang, X.; Chen, T. Evaluation on covalent and noncovalent linking of peptide to graphene oxide for MMP-9 detection. *Fullerenes, Nanotubes, Carbon Nanostruct.* **2018**, *26*, 38−41.
(14) Xu, S.; Zhan, J.; Man, B.; Jiang, S.; Yue, W.; Gao, S.; Guo, C.; Liu, H.; Li, Z.; Wang, J.; Zhou, Y. Real-time reliable determination of binding kinetics of DNA hybridization using a multi-channel graphene biosensor. *Nat. Commun.* **2017**, *8*, 14902.
(15) Andoy, N. M.; Filipiak, M. S.; Vetter, D.; Gutiérrez-Sanz, Ó.; Tarasov, A. Graphene-Based Electronic Immunosensor with Femtomolar Detection Limit in Whole Serum. *Adv. Mater. Technol.* **2018**, *3*, 1800186.
(16) Viswanathan, S.; Narayanan, T. N.; Aran, K.; Fink, K. D.; Paredes, J.; Ajayan, P. M.; Filipek, S.; Miszta, P.; Tekin, H. C.; Inci, F.; Demirci, U.; et al. Graphene-protein field effect biosensors: Glucose sensing. *Mater. Today* **2015**, *18*, 513−522.
(17) Jang, S. K.; Jang, J.-R.; Choe, W.-S.; Lee, S. Harnessing denatured protein for controllable bipolar doping of a monolayer graphene. *ACS Appl. Mater. Interfaces* **2015**, *7*, 1250−1256.
(18) Liu, S.; Fu, Y.; Xiong, C.; Liu, Z.; Zheng, L.; Yan, F. Detection of Bisphenol A Using DNA-Functionalized Graphene Field Effect Transistors Integrated in Microfluidic Systems. *ACS Appl. Mater. Interfaces* **2018**, *10*, 23522−23528.
(19) Tuteja, S. K.; Ormsby, C.; Neethirajan, S. Noninvasive Label-Free Detection of Cortisol and Lactate Using Graphene Embedded Screen-Printed Electrode. *Nano-Micro Lett.* **2018**, *10*, 41.
(20) Kim, K. S.; Lim, S. R.; Kim, S.-E.; Lee, J. Y.; Chung, C.-H.; Choe, W.-S.; Yoo, P. J. Highly sensitive and selective electrochemical cortisol sensor using bifunctional protein interlayer-modified graphene electrodes. *Sens. Actuators, B* **2017**, *242*, 1121−1128.
(21) Gao, W.; Chen, Y.; Xi, J.; Lin, S.; Chen, Y.; Lin, Y.; Chen, Z. A novel electrochemiluminescence ethanol biosensor based on tris(2,2′-bipyridine) ruthenium (II) and alcohol dehydrogenase immobilized in graphene/bovine serum albumin composite film. *Biosens. Bioelectron.* **2013**, *41*, 776−782.
(22) Zhou, L.; Wang, K.; Sun, H.; Zhao, S.; Chen, X.; Qian, D.; Mao, H.; Zhao, J. Novel Graphene Biosensor Based on the Functionalization of Multifunctional Nano-bovine Serum Albumin for the Highly Sensitive Detection of Cancer Biomarkers. *Nano-Micro Lett.* **2019**, *11*, 20.
(23) Forsyth, R.; Devadoss, A.; Guy, O. Graphene Field Effect Transistors for Biomedical Applications: Current Status and Future Prospects. *Diagnostics* **2017**, *7*, 45.
(24) Kaisti, M. Detection principles of biological and chemical FET sensors. *Biosens. Bioelectron.* **2017**, *98*, 437−448.
(25) Goda, T.; Miyahara, Y. Interpretation of protein adsorption through its intrinsic electric charges: A comparative study using a field-effect transistor, surface plasmon resonance, and quartz crystal microbalance. *Langmuir* **2012**, *28*, 14730−14738.
(26) Andronescu, C.; Schuhmann, W. Graphene-based field effect transistors as biosensors. *Curr. Opin. Electrochem.* **2017**, *3*, 11−17.
(27) Meléndrez, D.; Jowitt, T.; Iliut, M.; Verre, A. F.; Goodwin, S.; Vijayaraghavan, A. Adsorption and binding dynamics of graphene-supported phospholipid membranes using the QCM-D technique. *Nanoscale* **2018**, *10*, 2555−2567.
(28) Sauerbrey, G. Verwendung von Schwingquarzen zur Wä gung dünner Schichten und zur Mikrowä gung. *Z. Phys. Chem.* **1959**, *155*, 206−222.
(29) Jason-Moller, L.; Murphy, M.; Bruno, J. Overview of Biacore Systems and Their Applications. *Curr. Protoc. Protein Sci.* **2006**, *45*, 19.13.1−19.13.14.
(30) Su, J.; Esmaeilzadeh, H.; Zhang, F.; Yu, Q.; Cernigliaro, G.; Xu, J.; Sun, H. An ultrasensitive micropillar-based quartz crystal microbalance device for real-time measurement of protein immobilization and protein-protein interaction. *Biosens. Bioelectron.* **2018**, *99*, 325−331.
(31) Vashist, S. K.; Vashist, P. Recent Advances in Quartz Crystal Microbalance-Based Sensors. *J. Sens.* **2011**, *2011*, 1.
(32) Renart, J.; Behrens, M. M.; Fernández-Renart, M.; Martinez, J. L. Immunoblotting Techniques. *Immunoassay* **1996**, 537−554.
(33) Vashist, S. K.; Luong, J. H. T., "Immunoassays," *Handbook of Immunoassay Technologies*; Academic press: pp. 1−18, 2018.
(34) Huang, B.; Wang, L.; Zhang, Y.; Zhang, J.; Zhang, Q.; Xiao, H.; Zhou, B.; Sun, Z.; Cao, Y. N.; Chen, Y.; Hu, Z.; et al. A novel Time-resolved Fluoroimmunoassay for the quantitative detection of Antibodies against the Phospholipase A2 Receptor. *Sci. Rep.* **2017**, *7*, 1−8.
(35) Fresquet, M.; Jowitt, T. A.; Gummadova, J.; Collins, R.; O'Cualain, R.; McKenzie, E. A.; Lennon, R.; Brenchley, P. E. Identification of a major epitope recognized by PLA2R autoantibodies in primary membranous nephropathy. *J. Am. Soc. Nephrol.* **2015**, *26*, 302−313.
(36) Fresquet, M.; Jowitt, T. A.; McKenzie, E. A.; Ball, M. D.; Randles, M. J.; Lennon, R.; Brenchley, P. E. PLA2R binds to the annexin A2-S100A10 complex in human podocytes. *Sci. Rep.* **2017**, *7*, 6876.
(37) Glassock, R. J. The Pathogenesis of Idiopathic Membranous Nephropathy: A 50-Year Odyssey. *Am. J. Kidney Dis.* **2010**, *56*, 157−167.
(38) Hanko, J. B.; Mullan, R. N.; O'Rourke, D. M.; McNamee, P. T.; Maxwell, A. P.; Courtney, A. E. The changing pattern of adult primary glomerular disease. *Nephrol., Dial., Transplant.* **2009**, *24*, 3050−3054.
(39) Qin, W.; Beck, L. H., Jr.; Zeng, C.; Chen, Z.; Li, S.; Zuo, K.; Salant, D. J.; Liu, Z. Anti-Phospholipase A2 Receptor Antibody in Membranous Nephropathy. *J. Am. Soc. Nephrol.* **2011**, *22*, 1137−1143.
(40) Waldman, M.; Austin III, H. A. Controversies in the treatment of idiopathic membranous nephropathy. *Nat. Rev. Nephrol.* **2009**, *5*, 469−479.
(41) McGrogan, A.; Franssen, C. F. M.; de Vries, C. S. The incidence of primary glomerulonephritis worldwide: a systematic review of the literature. *Nephrol. Dial. Transplant.* **2011**, *26*, 414−430.
(42) Ponticelli, C. Membranous nephropathy. *J. Nephrol* **2007**, *20*, 268−287.
(43) Malmström, J.; Agheli, H.; Kingshott, P.; Sutherland, D. S. Viscoelastic modeling of highly hydrated laminin layers at homogeneous and nanostructured surfaces: Quantification of protein layer properties using QCM-D and SPR. *Langmuir* **2007**, *23*, 9760−9768.
(44) Huang, R.; Yi, P.; Tang, Y. Probing the interactions of organic molecules, nanomaterials, and microbes with solid surfaces using quartz crystal microbalances methodology, advantages, and limitations. *Environ. Sci. Process. Impacts* **2017**, *19*, 793−811.

(45) Mauro, M.; Zainuddin, A. A.; Nordin, A. N.; Rahim, R. A., "*openQCM verfication test using Impedance and Network Analyzer*," no. August, p. 5, 2016, DOI: 10.13140/RG.2.2.29417.29282.
(46) Hummers, W. S., Jr.; Offeman, R. E. Preparation of Graphitic Oxide. *J. Am. Chem. Soc.* **1958**, *80*, 1339−1339.
(47) Mauchauffé, R.; Moreno-Couranjou, M.; Boscher, N. D.; Van De Weerdt, C.; Duwez, A. S.; Choquet, P. Robust bio-inspired antibacterial surfaces based on the covalent binding of peptides on functional atmospheric plasma thin films. *J. Mater. Chem. B* **2014**, *2*, 5168−5177.
(48) Hamilton, P.; Kanigicherla, D.; Hanumapura, P.; Walz, L.; Kramer, D.; Fishcer, M.; Brenchley, P.; Mitra, S. Peptide GAM Immunoadsorption Therapy in Primary Membranous Nephropathy (PRISM): Phase II Trial Investigating the Safety and Feasibility of Peptide GAM Immunoadsorption in anti-PLA 2 R Positive Primary Membranous Nephropathy. *J. Clin. Apher.* **2018**, *33*, 283−290.
(49) Rodriguez-Pardo, L.; Farina, J.; Gabrielli, C.; Perrot, H.; Brendel, R. "Noise and resolution in 2 MHz, 6 MHz, 9 MHz and 27 MHz QCM sensors in liquid media," in *Proceedings of IEEE Sensors 2003 (*IEEE *Cat. No.03CH37498)*, pp. 1189−1193, DOI: 10.1109/ICSENS.2003.1279133.
(50) Sota, H.; Yoshimine, H.; Whittier, R. F.; Gotoh, M.; Shinohara, Y.; Hasegawa, Y.; Okahata, Y. A versatile planar QCM-based sensor design for nonlabeling biomolecule detection. *Anal. Chem.* **2002**, *74*, 3592−3598.
(51) Kanigicherla, D.; Gummadova, J.; McKenzie, E. A.; Roberts, S. A.; Harris, S.; Nikam, M.; Poulton, K.; McWilliam, L.; Short, C. D.; Venning, M.; Brenchley, P. E. Anti-PLA2R antibodies measured by ELISA predict long-term outcome in a prevalent population of patients with idiopathic membranous nephropathy. *Kidney Int.* **2013**, *83*, 940−948.
(52) Keiji Kanazawa, K.; Gordon II, J. G. The oscillation frequency of a quartz resonator in contact with liquid. *Anal. Chim. Acta* **1985**, *175*, 99−105.
(53) Kanazawa, K. K.; Gordon, J. G. Frequency of a Quartz Microbalance in Contact with Liquid. *Anal. Chem.* **1985**, *57*, 1770−1771.
(54) Zhang, Q.; Huang, B.; Liu, X.; Liu, B.; Zhang, Y.; Zhang, Z.; Hua, J.; Fan, Y.; Hu, L.; Meng, M.; Wu, M.; et al. Ultrasensitive Quantitation of Anti-Phospholipase A2 Receptor Antibody as A Diagnostic and Prognostic Indicator of Idiopathic Membranous Nephropathy. *Sci. Rep.* **2017**, *7*, 1−7.
(55) EUROIMMUN AG, "*Autoantibodies against phospholipase A2 receptor and THSD7A − EUROIMMUN*; EUROIMMUN: 2019. .
(56) Biolin Scientific, "*Qsensor QSX 301 Gold*; Biolin Scientific AB: 2018

https://dx.doi.org/10.1021/acssensors.0c01641
ACS Sens. 2020, 5, 3520−3532